Seismic Performance Assessment for Serviceability of Geosynthetic Reinforced Embankments

Ali RamazanBorujerdi[1]

[1] *Academic Instructor, Department of Civil Engineering,*
   Qom University of Technology, Tehran, 1651958171, IRAN

*Corresponding Author: aliborujerdi1371@gmail.com
DOI: https://doi.org/10.30880/emait.2024.05.01.006

Abstract

Embankments in the field of civil engineering were historically not given much attention in terms of their ability to withstand seismic activity, as they were considered to be non-critical structures. However, in recent years, the seismic stability of embankments has gained increasing importance in the field of geotechnical engineering. This increased significance is due to the need to quickly restore functional infrastructure after earthquakes. The occurrence of lateral spreading, resulting from foundation liquefaction, is the primary factor leading to embankment distress in geotechnical engineering during seismic events. To address this issue, this study presents a novel approach that employs geosynthetic basal reinforcement. The research paper presents a technique that uses geosynthetic basal reinforcement to manage the lateral spreading of embankments both pre- and post-earthquakes, guaranteeing their ongoing effectiveness. The proposed approach utilizes a pseudo-static limit equilibrium method for determining the tensile load produced in the basal reinforcement. The serviceability criteria establish the maximum strain permitted in the basal reinforcement by imposing a restriction on the horizontal movement of the embankment toe. By taking into account the tensile load of the reinforcement and the maximum allowable strain, it is feasible to establish an appropriate geosynthetic reinforcement that considers various factors including tensile strength, strain, design life, installation, and durability impacts.

1. Introduction

In order to assess the magnitude and duration of an earthquake, it is important to take into account the effects of earthquake load on embankments. It is crucial to consider the expected changes in embankment shear strength and deformation that occur during and immediately after an earthquake, as well as the potential instability of slopes caused by aftershocks and the loss of maintainability. Fig. 1 demonstrates the instability of different slopes due to earthquake loads, as reported by [1–6]. These extend to the surface sliding of the embankment (Fig. 1a), To create a sliding surface within the embankment (Fig. 1b), Regarding the generation of sliding surfaces due to unstable foundations (Fig. 1c), Embankment deflection and lateral spreading on unstable foundations are initiated (Fig. 1d). Figs. 1a and 2 illustrate that the foundation remains stable despite instability, which occurs solely inside an embankment.

Fig. 2 illustrates the application of foundation reinforcement to increase stability and reduce the lateral extent of embankments when it is subjected to seismic loads. A decrease in strength is caused by seismic loading here, Liquefaction of the foundation layer causes lateral displacement, which ultimately leads to the embankment's collapse. The shear strength of the liquefied base layer evolves through several stages: initially

defined by the $\varphi_{,p}$ conditions before the earthquake loading, then transitioning to the residual shear resistance Sr at liquefaction, and finally reaching the critical state shear strength $\varphi_{,cv}$ once equilibrium is re-established. Changes in foundation shear strength conditions can lead to instability of the embankment, which can be prevented by reinforcement and lateral spread. The approach presented in this research presupposes that the liquefaction occurs solely at the foundation, without any elevation of the groundwater table in the embankment, which may result in resorption inside the embankment.
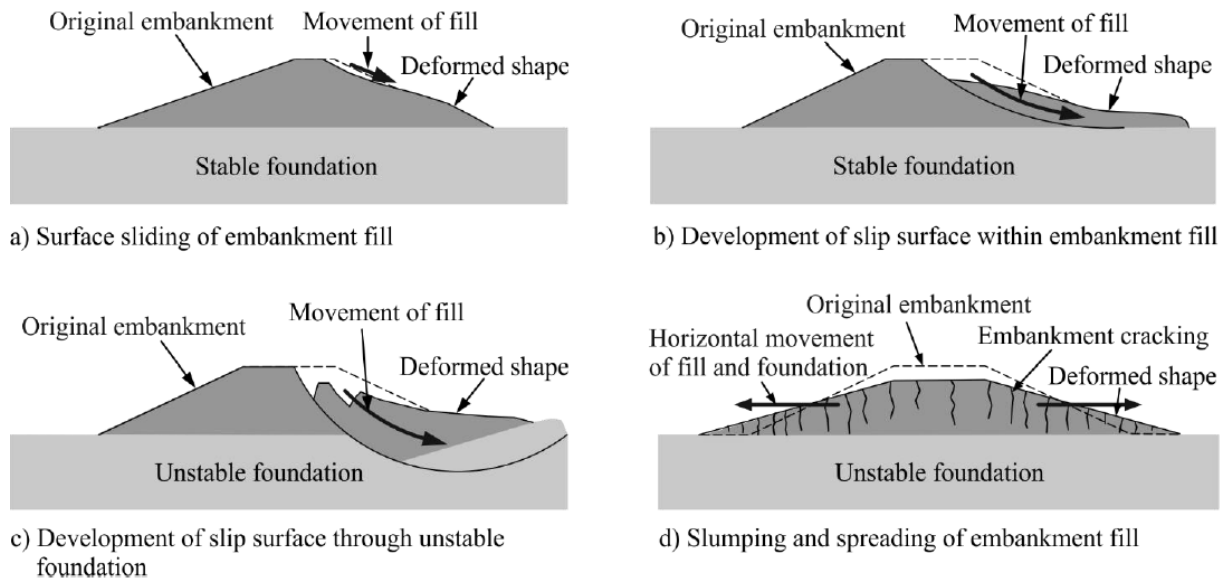

Fig. 1 *Various types of instability in slopes can result from earthquake loads*
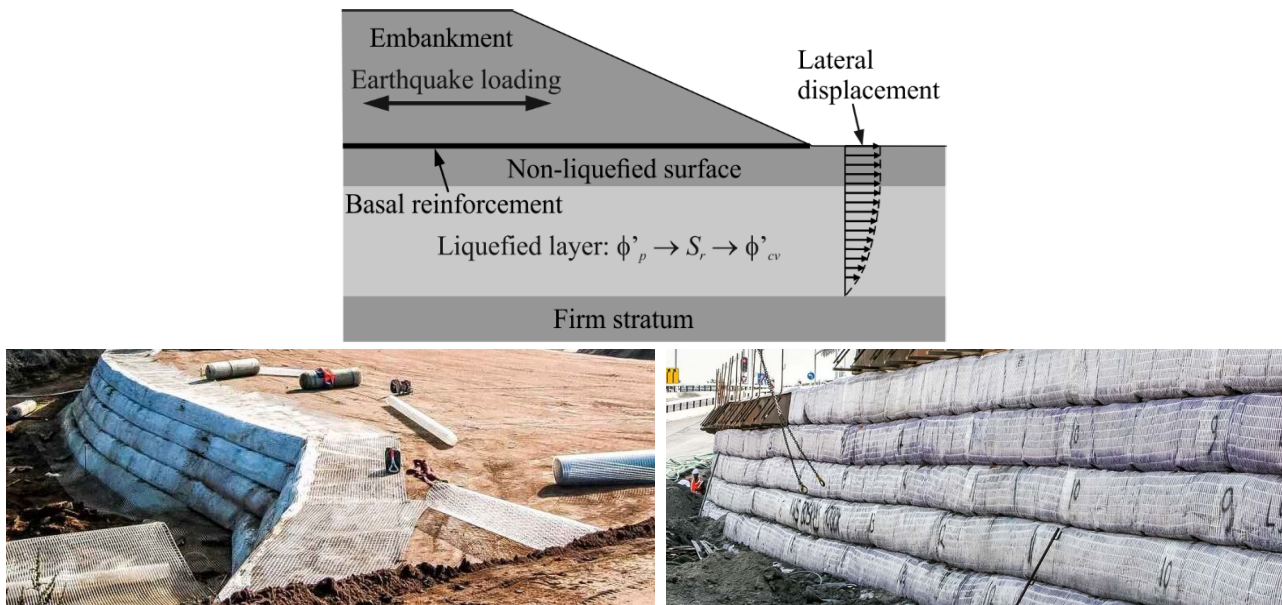

Fig. 2 *Embankments reinforcement to prevent instability and lateral spreading*

2. Liquefaction of Embankment

The liquefaction caused by earthquakes is linked to the reduction of the soil's strength and stiffness, leading to significant excess pore pressures and substantial soil deformations. Depending on the slope load, shape (slope) of the liquefied layer and its in-site density, as well as the level of water table, the severity of this process and the ground deformation it generates is determined by the type of melted layer with in–situ density. Saturated recent sand deposits with low to moderate field densities are most susceptible to liquefaction, but silty sands, sandy silts, and gravelly sands are also susceptible to liquefaction.

The length of an earthquake's duration ranges from 5 seconds to over 2 minutes, depending on the situation. In general, powerful earthquakes have a prolonged duration. Slope instability can be attributed to the initial earthquake shock, but there is also the possibility of earthquake aftershocks that cause instability and worsen the original condition. The most significant damage toe embankments has been caused by liquefaction events, which can occur after earthquakes of short or long duration [7–9].

The design of a slope on liquefiable base layers involves taking into account the susceptibility to liquidation and the residual shear strength that may occur after lithification. Several techniques have been created to gauge the foundation's liquefaction potential and residual shear strength. According to [10–13] the vulnerability of foundation layers to liquefaction can be determined using SPT and CPT tests, and they also mention a connection between these methods. Sr is the measure of residual shear strength in liquefied soil. Measures for embankments design to mitigate the risk of liquefaction on the ground can range from shifting the embankment to suitable ground improvement. These methods seem to be very costly. Fig. 3 and Fig. 4 show features of a simplified SPT and CPT system.
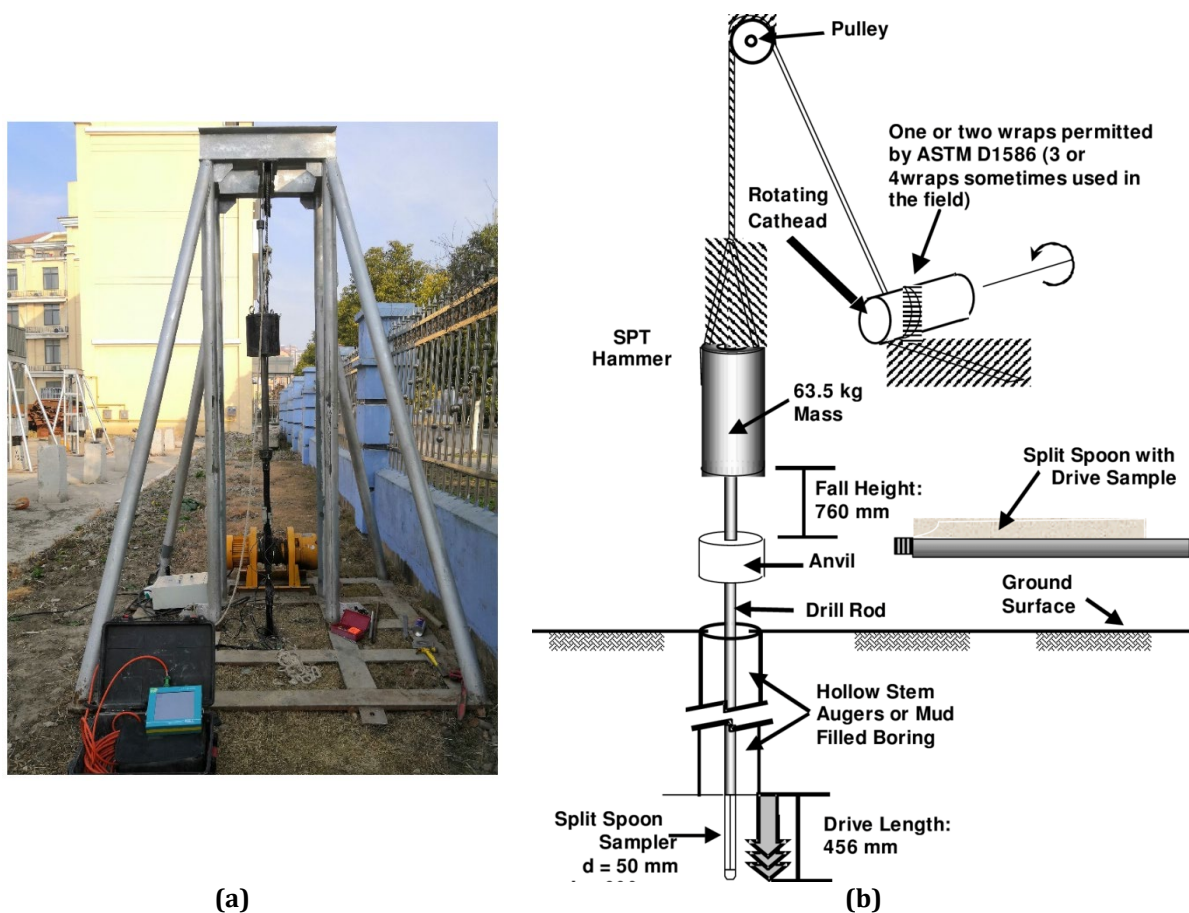

(a)   **(b)**

Fig. 3 *(a) Setup and Equipment for the Standard Penetration Test (SPT); (b) Schematic drawing of the instrumented SPT*

The thickness of the unliquefied surface layer (H1 in Fig. 5a) significantly affects the shape and extent of embankment instability. When the surface layer is substantial, with H1 exceeding 3 meters, the embankment typically remains stable and unaffected by foundation liquefaction because the thick surface layer can mitigate the effects of liquefaction [14–17]. When the surface layer is substantial, specifically with 2 m < H1 < 3 m, embankment instability manifests as lateral movement. This occurs due to the lateral deformations in the liquefied foundation layer being transmitted to the ground surface, as illustrated in Fig. 5a. This results in a horizontal expansion of the embankment. When there is a surface layer that is between 1 m and 2 m thick, slope instability is characterized by both lateral movement and rotational failure. These factors are influenced by the condition of the surface layer, as shown in Fig. 5b. Sand boils may appear on the soil surface, which can lead to a loss of surface integrity. On the other hand, if the surface layer is thin or nonexistent, with a depth less than 1 m, embankment instability is seen as rotational failure without any involvement from the surface layer, as depicted in Fig. 5c. The presence and potential damage caused by the non-liquefied surface layer during liquefaction depend on how far the embankment extends laterally.
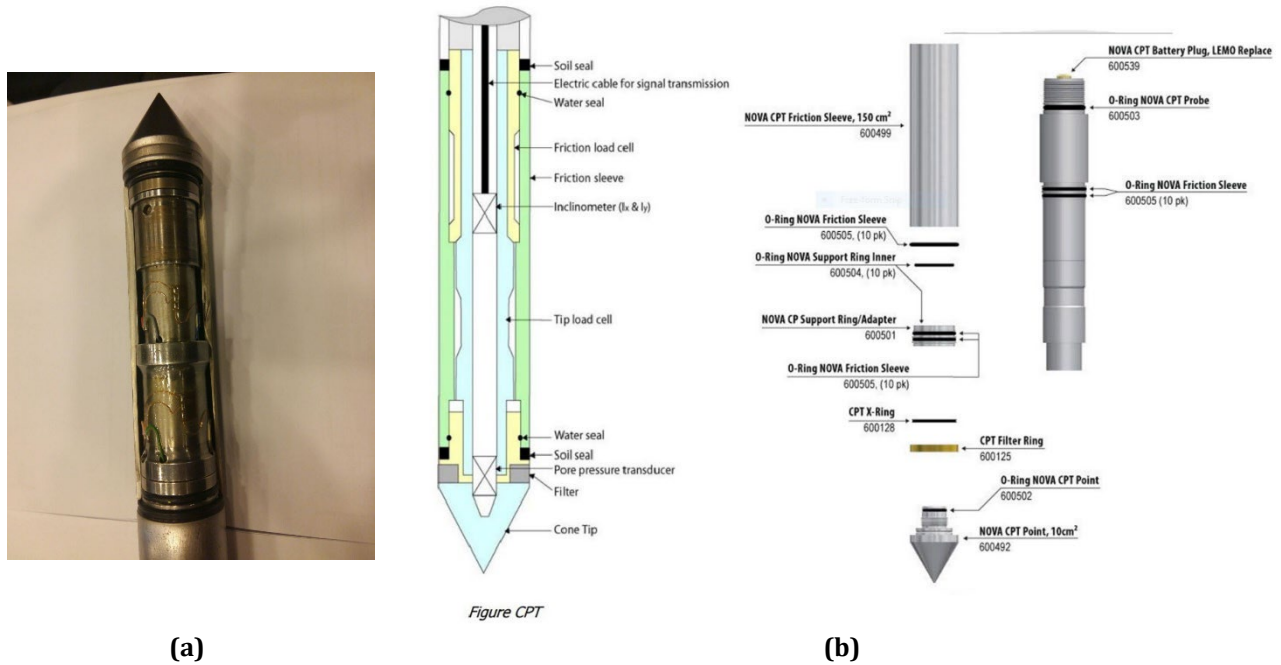
(a) **(b)**

Fig. 4 *(a) Setup and Equipment for the Cone Penetrometer Test (CPT); (b) Schematic drawing of the instrumented CPT*

It should be noted that the slope can undergo significant lateral expansion due to all three types of instability in Fig. 5. A straightforward method of analysing Figs. 5a and 5b can be used to focus on horizontal loads and deformations. A more complicated case of rotational failure is illustrated in Fig. 5c, which involves the examination of both vertical and horizontal loads and deformations.
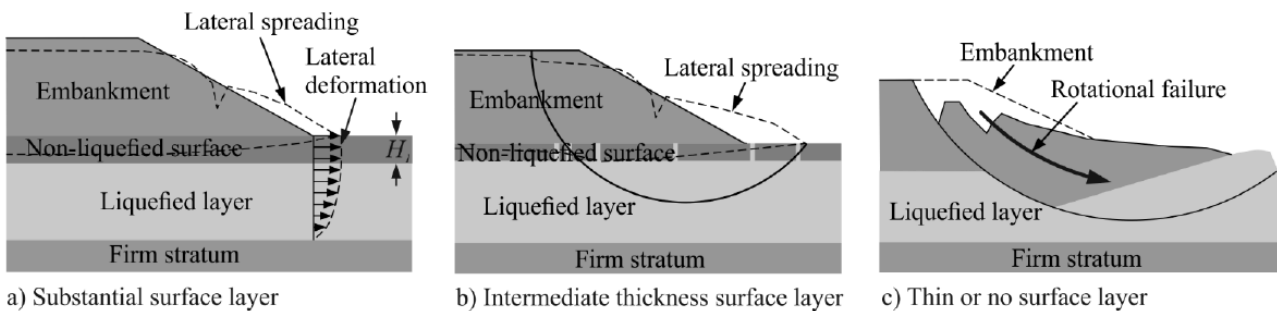

Fig. 5 *The extent and shape of slope instability are influenced by the thickness of the non-liquefied surface layer*

3. Application of Reinforcement to Limit The Lateral Spread of Embankments

Geosynthetic reinforcement has been utilized for decades to ensure the stability of embankments built on soft terrain. In the event that the embankment foundation is liquefied by seismic loads, the purpose of reinforcing it remains unchanged, with an initial goal of maintaining the stability of the structure and limiting horizontal displacement until the foundation stabilizes sufficiently to support the embankment. Geotechnical structures are often affected by seismic loads, which is why the pseudo-static limit equilibrium approach has been used and yielded reasonable results up to this point. This method takes into consideration the impact of earthquakes by utilizing a horizontal seismic coefficient, k_h, (refer to Fig. 6) in relation to the weight of the embankment side slope, W. Typically, the value of k_h is calculated as a percentage of the Peak Ground Acceleration (PGA) at the specific site. Various guidance documents recommend that k_h ranges from 20% to 100% of the PGA. The wide range of recommended values has caused confusion and excessive caution in the selection of k_h for pseudo-static analyses. Recently, more logical procedures have been developed to determine the appropriate values of k_h [19] and [20].
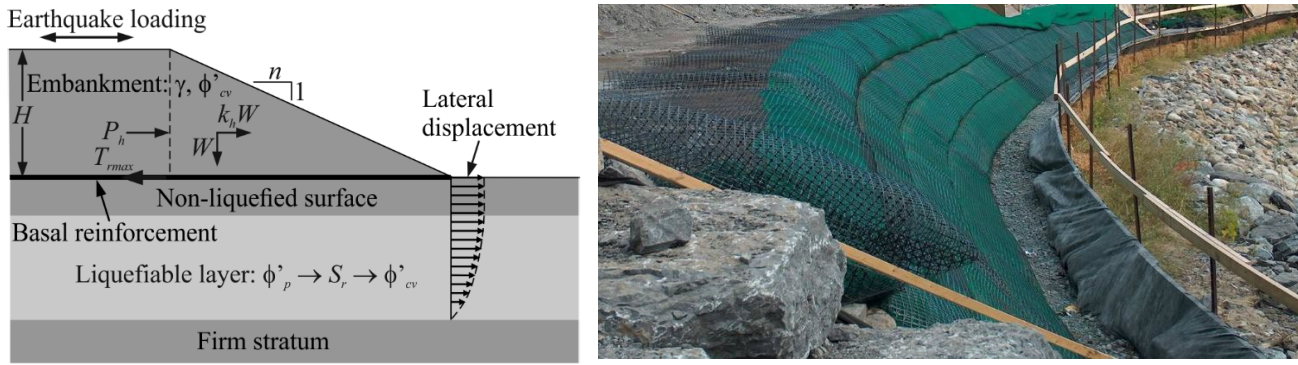
Fig. 6 *Pseudo-static limit equilibrium method for determining the basal reinforcement load during and after earthquake events.*

During and immediately after seismic loading, geosynthetic reinforcement is used to control the sideways movement of an embankment, as depicted in Fig. 6. When determining the shape of an embankment, it is common to consider the inclusion of peak shear strength parameters (φ,p) of the liquefiable base layer during periods of static equilibrium. However, seismic loading at some point along the slope can reduce shear strength of liquefiable layer to residual value S_r. The foundation's shear strength may be lost due to slope loading, resulting in significant lateral displacements until the liquefiable layer returns to its critical shearing state φ'_{cv}. Throughout the reinforcement process, the objective is to uphold the stability of the embankment and hinder any lateral movement of the embankment toe beyond a safe threshold.

If the predominant directional instability of the slope is horizontal (outward) in nature (Fig. 5a and 5b), such as when a significant non-liquefied surface layer is present (Fig. 5a and 5b), it is difficult to withstand at the base during an earthquake. Once the reinforcement is generated, T_{rmax} can be calculated as follows:

$$T_{rmax} = \frac{1}{2}\gamma H^2 \left\{ tan^2\left(\frac{\pi}{4} - \frac{Q'_{cv}}{2}\right) + K_h{}^n \right\} \tag{1}$$

To prevent the reinforcement from being pulled out of the embankment during seismic loading, it is necessary to determine the required bond length of the reinforcement beyond the embankment failure plane (L_E).

$$L_E \geq \frac{f_p T_{rmax}}{2\gamma H\alpha' tanQ'_{cv}} \tag{2}$$

As shown in Fig. 6, α' represents the bond coefficient between the basal reinforcement and the surrounding soil, and f_p is the factor of safety against reinforcement pull-out, typically set at 1.3 or 1.5. In scenarios with little to no non-liquefied surface layer (Fig. 5c), a more sophisticated method, such as slip-circle stability analysis incorporating pseudo-static components, should be employed to determine T_{rmax}.

$$n \geq \frac{f_s tan^2\left(\frac{\pi}{4} - \frac{Q'_{cv}}{2}\right)}{\alpha' tanQ'_{cv} - f_s K_h} \quad \text{or} \quad n \geq \frac{f_s tan^2\left(\frac{\pi}{4} - \frac{Q'_{cv}}{2}\right)}{(1-K_v)\alpha' tanQ'_{cv} - f_s K_h} \tag{3}$$

The parameters shown in Fig. 7 include f_s, the factor of safety against sliding, typically set at 1.3 or 1.5. The left-hand side of Equation (3) addresses only the horizontal seismic coefficient when evaluating sliding resistance along the basal reinforcement. However, for a more conservative approach, it is recommended to consider both horizontal and vertical seismic coefficients, as depicted on the right-hand side of Equation (3).

To keep embankments in serviceable condition, their maximum horizontal toe displacements should be limited to 0.2 meters for embankments up to 4 meters in height, and 0.3 meters for those exceeding 4 meters. The bridge abutment embankments may need to have stricter limitations on leg displacement if there is a pile foundation nearby. Fig. 8 provides a visual representation of the required foot displacement for different rebar heights (H) and side slope length ratios (n), with an upper limit set. In most practical scenarios, the maximum allowable elongation for reinforcement is typically found to be between 2% and 5%. The pseudo-static reinforcement load (T_{rmax}) calculated using Equation (1) must correspond with the maximum allowable reinforcement strain shown in Fig. 8. This relationship is illustrated in Fig. 9. From this alignment, the design strength (T_D) for the basal reinforcement is established.
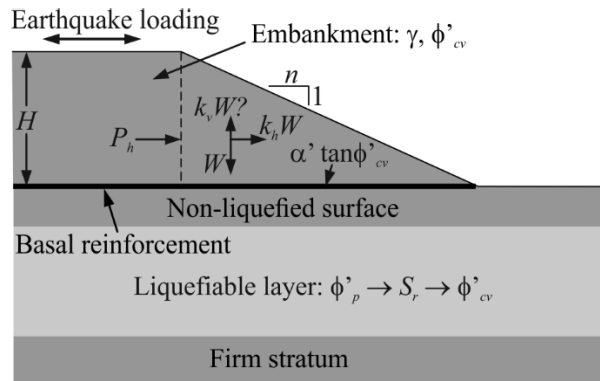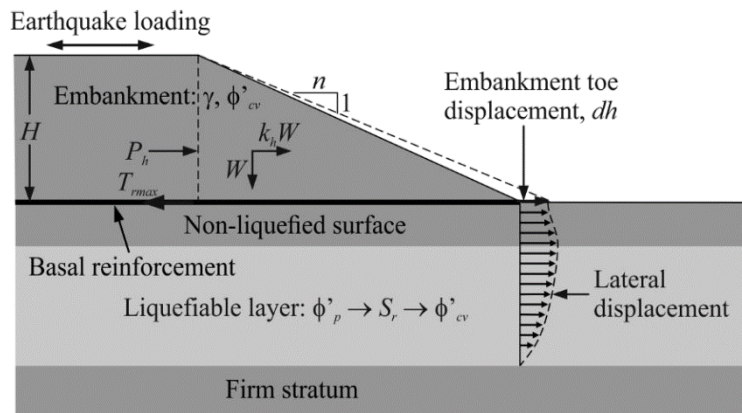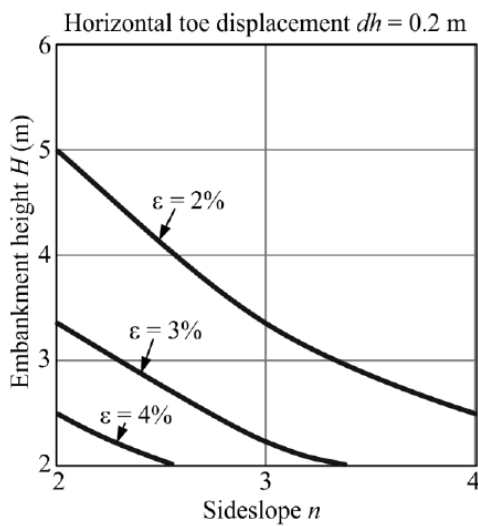
Fig. 7 *The parameters associated with Equation (3)*

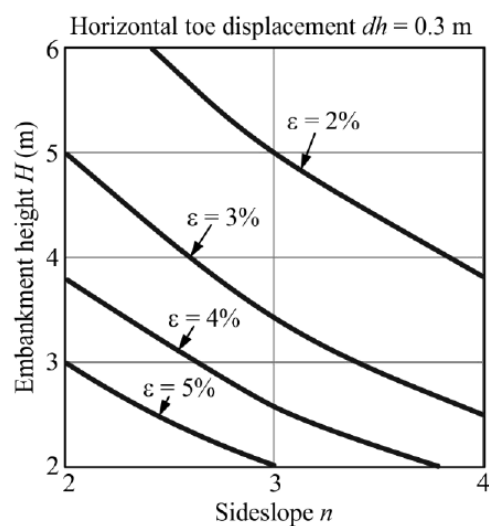$$T_D = \left(\frac{T_m}{T_{rmax}}\right) T_{rmax} \qquad (4)$$

T_m represents the strength of the reinforcement that is compatible with the reinforcement load T_{rmax} and the allowable reinforcement strain, as illustrated in Fig. 7.

(a) Maximum limit of tensile strain on reinforcement

(b)

(c)

Fig. 8 *Maximum allowable strain in basal reinforcement to control horizontal toe displacement*
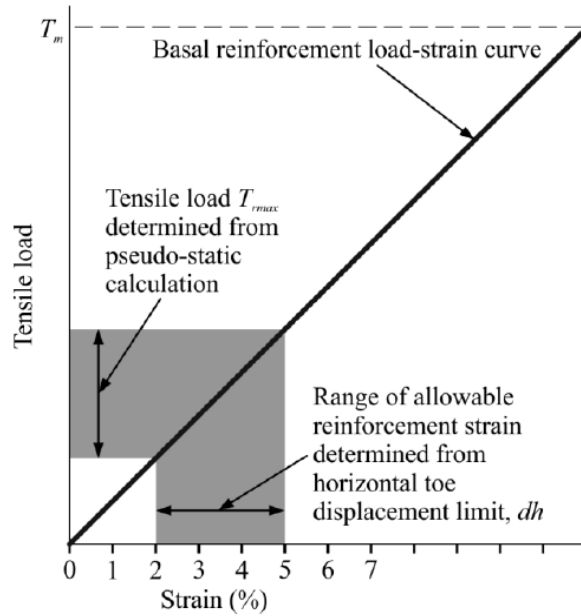
Fig. 9 *Maximum allowable strains and compatible reinforcement loads*

4. Reinforcement Load and Structural Strength Over Time

The basal reinforcement in this application acts as a precautionary measure in case of a design earthquake occurring at any point during the embankment's intended lifespan. As depicted in Fig. 10, an earthquake event could potentially happen at any time throughout the embankment's design life. From a design perspective, the most critical scenario occurs when the design earthquake loading occurs towards the end of the embankment's design life (at td in Fig. 10). In such cases, the design strength T_D of the reinforcement, determined by Equation (4), aligns with the in-situ strength of the reinforcement at the embankment's design life, t_d.

$$T_u = T_D(f_{id} \times f_{en})$$ (5)

The in-situ strength of reinforcement, T_i, at any point in time throughout the design lifespan of the embankment can be calculated as the characteristic initial tensile strength, T_u, divided by the reduction factor caused by installation damage, f_{id}, and further divided by the reduction factor due to environmental effects, f_{en}, as shown in Fig. 10. When reaching the design lifespan of the embankment, T_i is equal to T_D.

The three crucial performance properties for reinforcement are as follows:
- The specified lifespan of the base reinforcement design.
- The highest load capacity T_{rmax} at the maximum permissible strain for reinforcement.
- The initial tensile strength T_u that is characteristic of the reinforcement material.
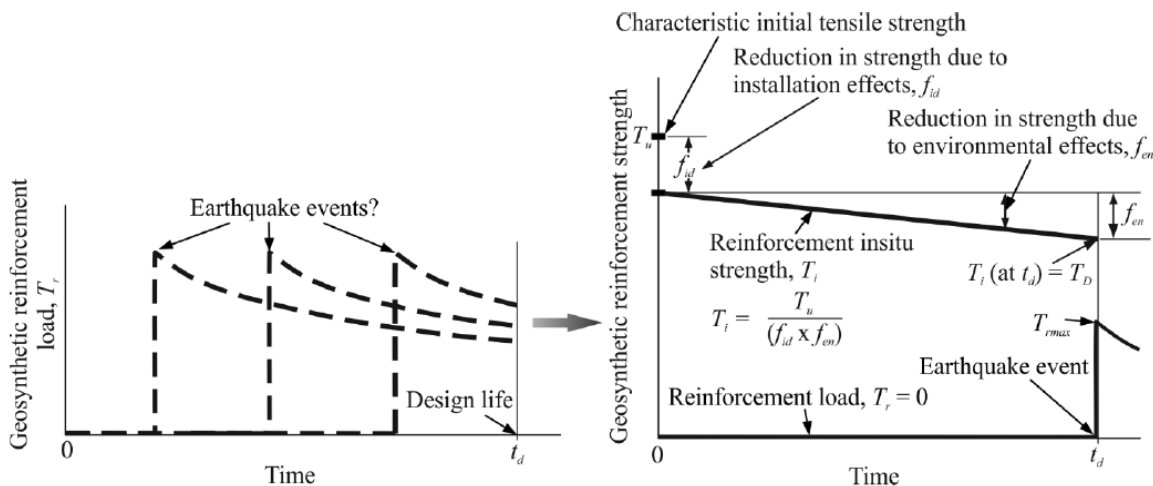

Fig. 10 *Principle of basal reinforcement load and design strength over time*

5. Conclusions

Geosynthetic basal reinforcement offers a cost-effective solution to mitigate embankment instability and lateral spreading both before and after seismic events. In this context, the basal reinforcement acts as a safeguard, maintaining the embankment's functionality even during liquefaction of the foundation layer caused by earthquakes. A method is provided for calculating the reinforcement load using pseudo-static analysis. By incorporating this with considerations of maximum allowable reinforcement strain to ensure the embankment's integrity, the necessary characteristics of the reinforcement's ultimate tensile strength can be determined. The critical phase for earthquake loading impacting basal reinforcement performance occurs when it coincides with the embankment's design life. An example is provided to illustrate how the required ultimate strength of the reinforcement is computed by integrating both reinforcement load and strain considerations to meet earthquake loading requirements and embankment design life criteria.

Acknowledgement

Conflict of Interest

Authors declare that there is no conflict of interests regarding the publication of the paper.

Author Contribution

The author confirms sole responsibility for the following: study conception and design, data collection, analysis and interpretation of results, and manuscript preparation.

References

[1]   Bartlett, S. F., & Leslie Youd, T. (1995). Empirical prediction of liquefaction-induced lateral spread. *Journal of Geotechnical Engineering*, *121*(4), 316–329. https://doi.org/10.1061/(ASCE)0733-9410(1995)121:4(316)

[2]   Bray, J. D., Sancio, R. B., Durgunoglu, T., Onalp, A., Youd, T. L., Stewart, J. P., Seed, R. B., Cetin, O. K., Bol, E., Baturay, M. B., Christensen, C., & Karadayilar, T. (2004). Subsurface Characterization at Ground Failure Sites in Adapazari, Turkey. *Journal of Geotechnical and Geoenvironmental Engineering*, *130*(7), 673–685. https://doi.org/10.1061/(asce)1090-0241(2004)130:7(673)

[3]   Bardet, J. P., Tobita, T., Mace, N., & Hu, J. (2002). Regional modeling of liquefaction-induced ground deformation. *Earthquake Spectra*, *18*(1), 19–46. https://doi.org/10.1193/1.1463409

[4]   Holzer, T. L., Bennett, M. J., Noce, T. E., Padovani, A. C., & Tinsley, J. C. (2006). Liquefaction hazard mapping with LPI in the Greater Oakland, California, area. *Earthquake Spectra*, *22*(3), 693–708. https://doi.org/10.1193/1.2218591

[5]   Hsein Juang, C., Yuan, H., Li, D. K., Yang, S. H., & Christopher, R. A. (2005). Estimating severity of liquefaction-induced damage near foundation. *Soil Dynamics and Earthquake Engineering*, *25*(5), 403–411. https://doi.org/10.1016/j.soildyn.2004.11.001

[6]   Lenz, J. A., & Baise, L. G. (2007). Spatial variability of liquefaction potential in regional mapping using CPT and SPT data. *Soil Dynamics and Earthquake Engineering*, *27*(7), 690–702. https://doi.org/10.1016/j.soildyn.2006.11.005

[7]   Borujerdi, A. R., & Sharahi, M. J. (2021). Seismic bearing capacity of strip footings adjacent to slopes using pseudo dynamic approach. *Mathematics and Computational Sciences*, *2*(1), 17–41. https://doi.org/10.30511/MCS.2021.137964.1009

[8]   Borujerd, A. R. (2023). Analysis of Geosynthetic – Reinforced Stone Piles – Supported Embankments. *Journal of Sustainable Underground Exploration*, *3*(1), 35–41. https://doi.org/10.30880/jsue.2023.03.01.006

[9]   Borujerdi, A. R. (2023). Site Characterization of Alluvial Silty Sand Soils by Dynamic In-Situ and Laboratory Tests. *International Journal of Sustainable Construction Engineering and Technology*, *14*(1), 260–269. https://doi.org/10.30880/ijscet.2023.14.01.023

[10]   Borujerdi, A. R. (2023). Numerical and Experimental Analysis of Seismic Soil Pile Structure Interaction. *Emerging Advances in Integrated Technology*, *3*(2), 1–10. https://doi.org/10.30880/emait.2022.03.02.001

[11]   Borujerdi, A. R., Jiriyaei Sharahi, M., & Amel Sakhi, M. (2019). Seismic displacement of Cohesive-friction slopes using Newmark method. *Proceedings of the 8th International Conference on Seismology and Earthquake Engineering (SEE8)*, 11–13. https://civilica.com/doc/1022403

[12]   Jiryaei, S. M., & Borujerdi, A. R. (2016). Upper-bound Solution for Seismic Bearing Capacity of Strip

Footings Near Slopes. *The 5th International Conference on Geotechnical Engineering and Soil Mechanics*. https://doi.org/10.1680/geot.2003.53.8.697

[13] Borujerdi, A. R., & Sharahi, M. J. (2019). Bearing Capacity of Footings Near Slopes. *Advance Researches in Civil Engineering*, *1*(1), 9–14. https://doi.org/10.6310/jog.201903_14(1).1

[14] Seed, H. B., & Idris, I. M. (1971). Simplified Procedure for Evaluating Soil Liquefaction Potential. *Journal of the Soil Mechanics and Foundations Division*, *97*(9), 1249–1273. https://doi.org/10.1061/jsfeaq.0001662

[15] Towhata, I., Sasaki, Y., Tokida, K. I., Matsumoto, H., Tamari, Y., & Yamada, K. (1992). Prediction of Permanent Displacement of Liquefied Ground by Means of Minimum Energy Principle. *Soils and Foundations*, *32*(3), 97–116. https://doi.org/10.3208/SANDF1972.32.3_97

[16] Youd, T. L., Hansen, C. M., & Bartlett, S. F. (2002). Revised Multilinear Regression Equations for Prediction of Lateral Spread Displacement. *Journal of Geotechnical and Geoenvironmental Engineering*, *128*(12), 1007–1017. https://doi.org/10.1061/(ASCE)1090-0241(2002)128:12(1007)

[17] Zhang, G., Robertson, P. K., & Brachman, R. W. I. (2004). Estimating Liquefaction-Induced Lateral Displacements Using the Standard Penetration Test or Cone Penetration Test. *Journal of Geotechnical and Geoenvironmental Engineering*, *130*(8), 861–871. https://doi.org/10.1061/(asce)1090-0241(2004)130:8(861)